Direct *K*-shell ionization probabilities in 30-MeV/u Ne- and 8.3-MeV/u C-induced reactions near zero impact parameter

V. L. Kravchuk, H. W. Wilschut, A. M. van den Berg, B. Davids, F. Fleurot, M. Hunyadi, M. A. de Huu, H. Löhner, and A. van der Woude
Kernfysisch Versneller Instituut, NL-9747AA Groningen, The Netherlands
(Received 6 December 2002; published 27 May 2003)

Direct *K*-shell ionization probabilities were measured in coincidence with elastically scattered particles in 30-MeV/u Ne+Sn, Tb, Pb, Th and 8.3-MeV/u C+Zr, Ag, Sn, Sm, Au, Pb, Th reactions. Experimental data were compared with calculations in the semiclassical approximation. The transitional behavior at the reduced velocity $\xi_K \approx 1$, where the projectile velocity approaches the velocity of the *K*-shell electrons, is discussed.

DOI: 10.1103/PhysRevA.67.052709 PACS number(s): 34.50.Fa, 29.30.Kv, 32.30.Rj, 25.70.−z

Many data already exist on the total ionization probability of *K*- and *L*-shell electrons in ion-atom collisions on light and heavy targets. Such data include a wide variety of ions ranging from protons to ^{40}Ar with bombarding energies from a few MeV/u to 80 MeV/u [1–3]. These total ionization cross sections are in a good agreement with theoretical predictions based on the plane-wave Born approximation, taking into account the corrections for binding-energy effects, Coulomb deflection, polarization, and relativistic effects [3]. In these studies, the deduced experimental ionization probabilities are integrated over impact parameter *b*.

It was already realized in the 1970s that it would be relevant to measure these probabilities as a function of the impact parameter, since such measurements would provide a much more sensitive test of the models used [4,5]. Small impact parameters experiments for the *L* shell have been performed using the fact that in an ion-atom collision the *K*-shell ionization takes place mainly at an impact parameter, which is small with respect to the radius of the *L* shell. The *L*-shell ionization probability is deduced from the energy shift or satellites of the *K* x ray due to *L*-shell vacancies. Such experiments have been performed for a large variety of projectiles and targets, see results of Refs. [6,7], and references therein. A measurement of the direct *K*-shell ionization probability near zero impact parameter can be performed by measuring in coincidence the elastically scattered projectile and the *K* x ray resulting from the filling of the hole in the *K*-shell or with the δ-electron emitted from the *K*-shell.

In our studies, we performed coincidence measurements between elastically scattered projectiles and *K* x rays. Impact parameters ranged from 39 fm in the 8.3-MeV/u C on Th to 17 fm in the 30 MeV/u-Ne on Sn, which are near zero on the atomic scale (*K*-shell radius $a_K = a_0/(Z_2 - 0.3)$, where $a_0 = 52\,900$ fm). In addition to their intrinsic interest, such data are also necessary for the interpretation of experiments in which the duration of nuclear processes, for instance nuclear fission initiated by a nuclear excitation process, is deduced by using the *K*-shell vacancy lifetime as a clock [8]. Such applications require that the ionization probability can be calculated reliably.

In this paper, we present *K*-shell ionization probabilities at small impact parameters obtained for 8.3 MeV/u-C ions [9] and 30 MeV/u-Ne ions on a range of heavy and medium mass targets. The main problem in these measurements is the small ionization probability, which necessitates the elimination of a large background due to the accidental coincidences between elastically scattered projectiles and *K* x rays. This can be achieved by a careful subtraction of the random spectrum from the prompt spectrum using coincident time correlation. In addition, the slight energy difference $\Delta E = E_B(K) + E(\delta)$ between the ionizing and nonionizing projectiles is helpful to distinguish in the subtracted spectrum the true events and those due to statistical fluctuations of the prompt and random spectra. Here, E_B is the binding energy of the *K*-shell electron and $E(\delta)$ is the kinetic energy of the emitted electron. The better the energy resolution of the detection system for the scattered particle, the better this energy shift can be exploited. Therefore, a magnetic spectrograph was used for the momentum analysis of the elastically scattered ionizing and nonionizing projectiles, as was done in our earlier work for 15-MeV protons and 50-MeV α particles on Pb atoms [10].

The experimental arrangement for the 8.3-MeV/u C experiment is similar to the one described in Ref. [10]. There, the ^{12}C beam with a current $\leqslant 20e$nA from the KVI AVF cyclotron was used to bombard ^{232}Th, ^{nat}Pb, ^{197}Au, ^{150}Sm, ^{120}Sn, ^{109}Ag, and ^{nat}Zr targets with thicknesses ranging from 80 to 200 μg/cm^2. The projectile scattered over angles of $(12° \pm 1.5°)$ were detected with the QMG/2 magnetic spectrograph [11] using a multiwire proportional chamber backed by a scintillator detector arrangement in the focal plane. The overall energy resolution was about 60 keV. Two small Ge x-ray detectors positioned at 90° with respect to the beam direction were used. The count rate due to *L* x rays was reduced by placing an Al absorber ranging in thickness from 0.4 to 2 mm between target and detectors. The overall photoefficiency was obtained by calibrating with standard radioactive sources of ^{241}Am, ^{152}Eu, ^{133}Ba, and ^{57}Co placed at the target position. The absolute ionization probability was obtained by comparing the yield of nonionizing with that of ionizing elastically scattered projectiles and by assuming an isotropic distribution of the x rays. Figure 1(a) shows a spectrum for the reaction Pb(^{12}C, ^{12}C′X)Pb at 8.3 MeV/u bombarding energy. The spectrum obtained by subtracting the random spectrum from the prompt spectrum is shown in Fig. 1(b). Characteristic errorbars and the *K*-shell binding energy

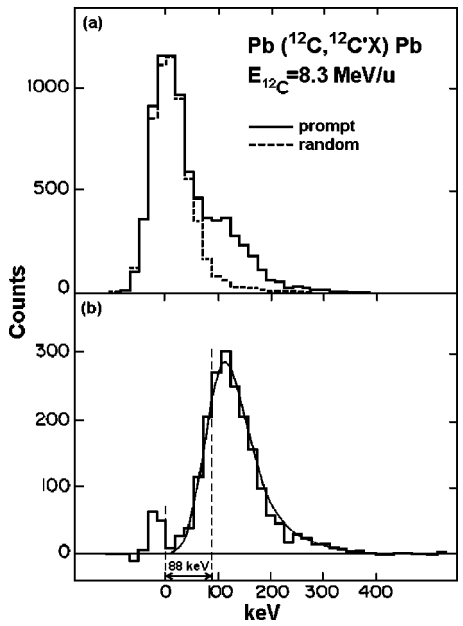

FIG. 1. (a) Taken from Ref. [9], shows the prompt and random particle spectra in the case of 8.3-MeV/u C scattered on Pb. (b) Shows the true spectrum resulting from subtracting the random spectrum from the prompt spectrum; characteristic errorbars are given and the *K*-shell binding energy of Pb, 88 keV, is indicated. The full curve in (b) is obtained by folding the theoretical distribution calculated in Ref. [12] with the experimental shape of the elastic peak. The calculation has been performed with hydrogenic wave functions in the united atom limit. The total ionization probability has been normalized to the experimental value.

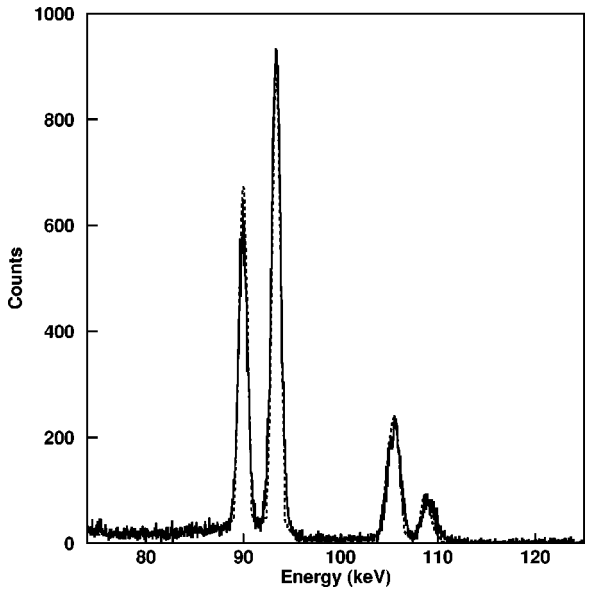

FIG. 2. True coincident *K* x-ray spectrum resulting from the reaction 30-MeV/u ^{20}Ne+^{232}Th. The solid line presents experimental and the dashed line presents fitted data ($\chi^2=1.2$).

are indicated. In this case, the energy resolution was good enough so that the spectrum thus obtained reflects the δ-electron energy spectrum. The full line results from folding the energy resolution of the particle detector system with the theoretical curve calculated by Trautmann and Rösel [12], normalized to the experimentally obtained total ionization probability. We also notice that a prompt-random subtraction is sufficient to obtain accurately the ionization probabilities. The probabilities are much larger than for proton and α-particle scatterings. Consequently, the momentum loss measurement is not necessary here.

The 30 MeV/u experiment was performed using a $^{20}Ne^{7+}$ beam from the superconducting cyclotron AGOR at KVI, Groningen. Targets were ^{232}Th, ^{208}Pb, ^{159}Tb, and ^{120}Sn with thicknesses of 4.8, 2.7, 1.0, and 0.2 mg/cm^2, respectively. Characteristic x rays were measured in coincidence with elastically scattered particles. The x rays were measured using two large 20 cm^2 area high-purity Ge planar x-ray detectors. The elastic reaction channel was identified using the Big-Bite Spectrometer (BBS) [13]. The BBS was set at 4°, considerably smaller than the grazing angles, which ranged between 7° (^{120}Sn), and 11° (^{232}Th). The Rutherford cross section at 4° ranges from 0.6 kb/sr (^{120}Sn) to 2.0 kb/sr (^{232}Th). The solid angle covered by the BBS is 9.2 msr. Elastically scattered Ne particles were registered using a detector system consisting of six phoswich detectors [14] positioned in the focal plane of the BBS. Data were accumulated to have about 10^4 true coincident x rays. Absolute efficiency measurements were made as described before. The Ge detectors were positioned at 135° with respect to the beam direction at a distance of 5 cm from the target. Al absorbers with thicknesses of 1 mm in the case of measurements with the ^{159}Tb and ^{120}Sn targets and 3 mm in case of the ^{232}Th and ^{208}Pb targets effectively removed the intense contribution of *L* x rays on the low-energy side of the spectrum. The count rate of x rays was about 3.5 kHz in each Ge detector, and for elastically scattered particles detected in the focal plane detectors about 160 kHz in total. A typical true coincident x-ray spectrum for ^{20}Ne+^{232}Th reaction is shown in Fig. 2. The prompt counts to random counts ratio was about 2:1. The absence of background above the highest-energy *K* x rays demonstrates the proper random subtraction of the nuclear γ rays from the prompt *K* x-ray spectra. The background at lower energies is due to the response of the x-ray detector. The absolute *K*-shell ionization probabilities were determined as the ratio of the number of true coincident *K* x rays to the number of elastically scattered particles taking into account the Ge x-ray detector efficiency. Due to the high statistics of x-ray and elastic counts, errors in this experiment are determined by the uncertainty in the efficiency of the Ge x-ray detectors and the target thickness.

The result of our ionization probability measurements near zero impact parameter is given in Tables I and II for the Ne and Carbon data, respectively. The tables also list the theoretical predictions (cf. Refs. [12,16]). These predictions are made in two distinct approximations. The first one is the united atom approximation (UA), where it is assumed that as the projectile penetrates the inner electronic shells, these shells adjust to reflect the increased binding of the combined projectile and target nuclear charge. When the projectile moves too fast to effect such a change and the *K* shell is assumed not to change, this is the separated atom approxi-

TABLE I. Theoretical and experimental direct *K*-shell ionization probabilities P_K in units of 10^{-3} for 30-MeV/u Ne projectiles. Calculations for the united atom (UA) and the separated atom (SA) approximations are given, including the corresponding reduced velocity ξ_K.

	UA		SA		Experiment	
Target	ξ_K	P_K	ξ_K	P_K	P_K	Error ΔP_K
^{232}Th	0.66	24.8	0.77	29.6	21	2
^{208}Pb	0.74	28.4	0.87	36.6	29	3
^{159}Tb	0.98	45.7	1.17	64.6	67	7
^{120}Sn	1.29	77.6	1.60	112.0	97	10

mation (SA). In either case, the relevant velocity is that of the projectile relative to the *K*-shell electron. This reduced velocity ξ_K is defined as

$$\xi_K(Z_2)=\frac{2}{\theta}\frac{v_p}{v_K}, \tag{1}$$

where v_p and v_K are the projectile and *K*-shell orbital electron velocities, respectively. $\theta(Z_2)=E_B(Z_2)/(Z_2-0.3)^2R$ is a screening parameter showing the nonhydrogenic character of the *K*-shell ionization energy, where $E_B(Z_2)$ is the *K*-shell binding energy and $R=13.6$ eV is the Rydberg constant. Z_2 is the effective atomic number of the target. In the UA approximation v_K, E_B, and θ use $Z_2=Z_{target}+Z_{projectile}$, while in the SA $Z_2=Z_{target}$ is used. Whereas for light projectiles the difference between the two predictions is small, for heavier projectiles the difference is quite strong, in particular, for Ne. The experimental results appear to indicate that around $\xi_K\approx 1$, a transition from the UA to the SA is required.

To investigate this transitional character in more detail, we show our results together with a compilation of other light-ion data under the assumption of the SA and UA in Figs. 3 and 4, respectively. The full triangles and full squares are from the 8.3-MeV/u C and 30-MeV/u Ne experiments, respectively. The ionization probabilities are normalized to

TABLE II. Theoretical and experimental direct *K*-shell ionization probabilities P_K in units of 10^{-3} for 8.3-MeV/u C projectiles. Calculations for the united atom (UA) and the separated atom (SA) approximations are given, including the corresponding reduced velocity ξ_K.

	UA		SA		Experiment	
Target	ξ_K	P_K	ξ_K	P_K	P_K	error ΔP_K
^{232}Th	0.37	2.23	0.41	2.50	1.8	0.3
^{208}Pb	0.42	2.67	0.46	3.24	2.3	0.3
^{197}Au	0.44	2.93	0.48	3.67	2.6	0.25
^{150}Sm	0.58	6.46	0.65	9.36	6.0	0.9
^{nat}Sn	0.74	14.3	0.85	22.5	25	8
^{109}Ag	0.79	17.9	0.91	28.5	32	20
^{nat}Zr	0.94	30.9	1.10	50.0	94	50

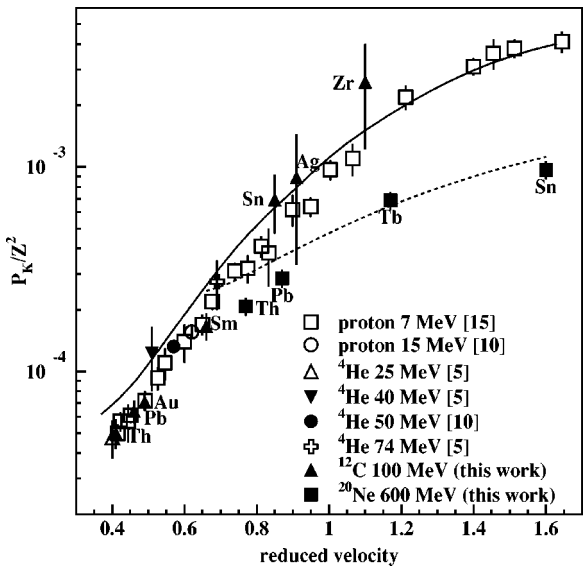

FIG. 3. The *K*-shell ionization probability, normalized to the square of the projectile atomic number, for C (full triangles) and Ne (full squares) ions determined from our experiments together with the data points from our earlier experiments for protons (open circle) and α particles (open triangle, full inverse triangle, full square, and open cross). Data points from [15] for protons (open squares) are also shown. The full curve is from a SCA calculation for the protons with relativistic hydrogenic wave functions and taking into account the increased binding. The dashed curve is the SCA for Ne at 30 MeV/nucleon in the SA approximation. The reduced velocity of the data points has been determined in the SA approximation as well.

the atomic number of the projectile, Z_1, using P_K/Z_1^2, which allows one to scale the light projectile data. (For the heavier projectiles, see below.)

The light-ion data we include are the results of our previous experiments on a Pb target for 15-MeV protons (open

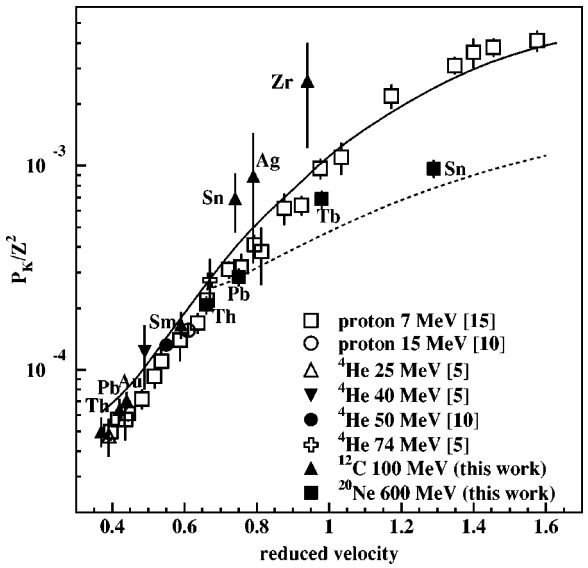

FIG. 4. Same data as in Fig. 3, but for the UA approximation.

circles), 25-MeV (open triangle), 40-MeV (full inverse triangle), 50-MeV (full circle), and 74-MeV (open cross) α particles, and the results of 7-MeV protons on various targets (open squares) [15].

The full curves results from a semiclassical approximation calculation scheme for protons as projectiles using relativistic hydrogenic wave functions in which recoil and increased binding effects have been taken into account [10,12]. The dashed curve represents the corresponding calculations for Ne [16]. The theoretical curves in the SA and UA plots are identical because the UA and SA are only distinguished by ξ_K. We note that the usual Z_1^2 scaling does not apply anymore for the Ne data and SCA calculations. The reason is that the adiabatic radius, i.e., where the ionization process is kinematically favored, becomes much larger than classical *K*-shell radius for lighter targets.

By observing the overall agreement between data and theory, it appears that the UA works best for $\xi<0.7$, while the SA appears to be appropriate for $\xi_K>1$. To see this quantitatively, we evaluated the χ^2 in 4 bins of ξ_K for the Ne, C, and He data. The result is shown in Fig. 5. The sharp change in χ^2 near $\xi_K=1$ indicates that the SA is most appropriate above and the UA below this value.

In conclusion, we have obtained different data on *K*-shell ionization probabilities for zero impact parameter collisions in a regime where the projectile velocity is of the same order as the *K*-shell electron velocity ($\xi_K\approx 1$). The data are in a good agreement with SCA calculations for different projectile-target combinations; in the separated atom approximation for $\xi_K>1$ and in the united atom approximation below this value.

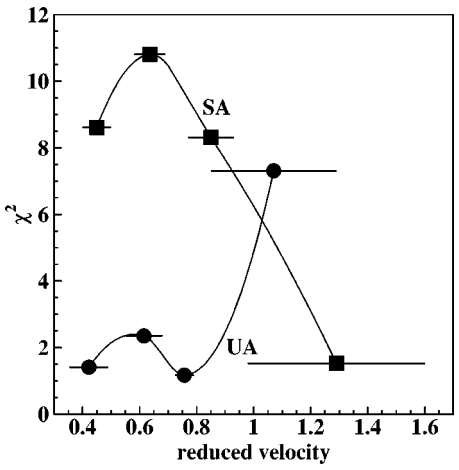

FIG. 5. $\chi^2=1/N-1\Sigma_i^N(P_{K_i}^{expt}-P_{K_i}^{theor})^2/(\Delta P_{K_i}^{expt})^2$. χ^2 has been evaluated for four bins in ξ_K for the SA and the UA approximations, respectively.

We would like to thank M. Polasik and D. Trautmann for performing the SCA calculations. This work has been performed as a part of the research program of the ''Stichting voor Fundamenteel Onderzoek der Materie'' (FOM), which is financially supported by the ''Nederlandse Organisatie voor Wetenschappelijk Onderzoek'' (NWO).

[1] V. Horvat, G. Sampoll, K. Wohrer, M. Chabot, and R.L. Watson, Phys. Rev. A **46**, 2572 (1992).
[2] D.F. Anagnastopoulos, G. Borchert, D. Gotta, K. Rashid, D.H. Jakubassa-Amundsen, and P.A. Amundsen, Phys. Rev. A **58**, 2797 (1998).
[3] V.L. Kravchuk, A.M. van den Berg, F. Fleurot, M.A. de Huu, H. Löhner, H.W. Wilschut, M. Polasik, M. Lewandowska-Robak, and K. Słabkowska, Phys. Rev. A **64**, 062710 (2001).
[4] E. Laegsgaard, J.U. Andersen, and L.C. Feldman, Phys. Rev. Lett. **29**, 1206 (1972).
[5] R.J. Vader, A. van der Woude, R.J. de Meijer, J.M. Hansteen, and P.A. Amundsen, Phys. Rev. A **14**, 62 (1976).
[6] E. Liatard, J.F. Bruandet, F. Glasser, Tsan Ung Chan, G.J. Costa, C. Gérardin, C. Heitz, M. Samri, and R. Seltz, Z. Phys. D: At., Mol. Clusters **2**, 223 (1986).
[7] M. Polasik, S. Raj, B.B. Dhal, H. Padhi, A.K. Saha, M.B. Kurup, K.G. Prasad, and P.N. Tandon, J. Phys. B **32**, 3711 (1999).
[8] Proposal R18, KVI, Groningen, 2000.
[9] J.H. van Dijk, Ph.D. thesis, Rijksuniversiteit Groningen, 1984 (unpublished).
[10] J.H. van Dijk, H.W. Wilschut, A.G. Drentje, and A. van der Woude, Z. Phys. A **314**, 1 (1983).
[11] A.G. Drentje, H.A. Enge, and S.B. Kowalski, Nucl. Instrum. Methods **122**, 485 (1974).
[12] D. Trautmann and F. Rösel, Nucl. Instrum. Methods **169**, 259 (1980).
[13] A.M. van den Berg, Nucl. Instrum. Methods Phys. Res. B **99**, 637 (1995).
[14] H.K.W. Leegte, E.E. Koldenhof, A.L. Boonstra, and H.W. Wilschut, Nucl. Instrum. Methods Phys. Res. A **313**, 26 (1992).
[15] M. Dost, S. Hoppenau, J. Kising, S. Röhl, and P. Schorn, Phys. Rev. A **24**, 693 (1981).
[16] M. Polasik and D. Trautmann (private communication).